Cell Stem Cell
Article

Potency and Fate Specification in CNS Stem Cell Populations In Vitro

Rea Ravin,[1,5] Daniel J. Hoeppner,[1,5] David M. Munno,[1] Liran Carmel,[2] Jim Sullivan,[1] David L. Levitt,[1] Jennifer L. Miller,[1] Christopher Athaide,[3] David M. Panchision,[4] and Ronald D.G. McKay[1,*]
[1]Laboratory of Molecular Biology, National Institute of Neurological Disorders and Stroke, National Institutes of Health, Bethesda, MD 20892, USA
[2]National Library of Medicine, National Institutes of Health, Bethesda MD 20894, USA
[3]EYE Biomachines, Houston, TX 77005, USA
[4]Center for Neuroscience Research, Children's Research Institute, Children's National Medical Center, Washington, DC 20010, USA
[5]These authors contributed equally to this work
*Correspondence: mckay@codon.nih.gov
DOI 10.1016/j.stem.2008.09.012

SUMMARY

To realize the promise of stem cell biology, it is important to identify the precise time in the history of the cell when developmental potential is restricted. To achieve this goal, we developed a real-time imaging system that captures the transitions in fate, generating neurons, astrocytes, and oligodendrocytes from single CNS stem cells in vitro. In the presence of bFGF, tripotent cells normally produce specified progenitors through a bipotent intermediate cell type. Surprisingly, the tripotent state is reset at each passage. The cytokine CNTF is thought to instruct multipotent cells to an astrocytic fate. We demonstrate that CNTF both directs astrogliogenesis from tripotent cells, bypassing two of the three normal bipotent intermediates, and later promotes the expansion of specified astrocytic progenitors. These results show how discrete cell types emerge from a multipotent cell and provide a strong basis for future studies to determine the molecular basis of fate specification.

INTRODUCTION

In spite of the great interest in the developmental potential of mammalian stem cells, there are very few studies where the precise logic and timing of fate choice has been defined. The presence of hematopoietic stem cells (HSCs) was first suggested by the ability of stem cells to form clonal colonies in the spleen and to reconstitute the murine hematopoietic system (Till et al., 1964). Immunosorting and functional reconstitution supports a developmental hierarchy in which stem cells generate terminal fates through discrete intermediate progenitors (Osawa et al., 1996; Spangrude et al., 1988; Weissman, 1994). However, many fundamental aspects of how HSCs generate terminal fates are still unresolved. These include the relative importance of intrinsic and extrinsic factors and the precise timing of the events in the commitment of HSCs to different fates (Ogawa, 1993).

A complete stem cell lineage remains to be determined for the hematopoietic system or any other mammalian tissue. In vitro cultures of telencephalic cortical neural stem cells give rise to neurons, astrocytes, and oligodendrocytes (Davis and Temple, 1994; Johe et al., 1996). Maintenance of the undifferentiated stem/progenitor cell is a significant unresolved issue in developmental biology and medicine. Lineage analysis of cells from the developing mouse telencephalon suggests that a cell-intrinsic asymmetric process regulates self-renewal and the production of discrete neuronal classes (Qian et al., 2000; Shen et al., 2006).

The lineage path from a single neural stem/progenitor cell to the production of neurons, astrocytes, and oligodendrocytes has never been established. The aim of this work is to define the discrete steps in producing a complex cell population from a single cultured cell. The technical challenges of long-term imaging in vivo prohibit the acquisition of complete lineages. The advantage of working on in vitro cultured samples is that direct access to each cell in a lineage may be possible. Further, the wide use of cultured CNS stem cells in research requires the accurate definition of changes in cell state through time. Most cell-based therapeutic applications will require expansion of primary cells in culture before grafting. For these reasons, it is critical to define the progression in cell state for cultured primary neural stem cells.

We developed an in vitro system that allows analysis of the transitions in fate from multipotent CNS stem cells to differentiated neurons and glia. The system includes a novel live-cell chamber, a method to restrict migration to the visual field and a methodology to determine the points of fate specification. In this work, we refer to cells that produce only one cell type as specified rather than committed (Slack, 1991).

We find that multipotent precursor (stem) cells are normally specified into discrete fates through the three possible bipotent intermediates that give rise to neurons+astrocytes (NA), neurons+oligodendrocytes (NO), and astrocytes+oligodendrocytes (AO). Using CNTF, a ligand widely used to produce astrocytes from neural stem cells, we show that instructive and selective effects regulate discrete intermediate cell types in astrogliogenesis. CNTF instructs tripotent cells to the astrocytic fate directly, bypassing the NA and AO bipotent intermediates, and later, CNTF promotes selective expansion of astrocytic precursors. These results demonstrate that through complete lineage

analysis, discrete cell types and transitions can be measured. The response of multipotent cells to environmental variables indicates that the mechanisms that specify distinct fates within the same cell are differentially sensitive.

RESULTS

Lineage Analysis

To obtain control cell lineages, we followed the development of neurons, astrocytes, and oligodendrocytes from single primary neural stem/progenitor cells derived from the embryonic day 14.5 (E14.5) rat telencephalon using time-lapse imaging. The rationale for developing a system around the E14.5 rat telencephalon is that significant numbers of neurons, astrocytes, and oligodendrocytes can be derived from single cells in clonal assays from this developmental stage (Johe et al., 1996). In the few previous studies that derive functional neurons from CNS stem cells, most required an astrocytic support cell (Blondel et al., 2000; Song et al., 2002; Vicario-Abejon et al., 1998). For the production of functional neurons, we used a strategy where CNS stem cells were plated and expanded in DMEM/F12 with the N2 supplement (hereafter referred to as N2) in the presence of bFGF for 3 days. Cell-cycle withdrawal was initiated by removing bFGF and culturing cells for 2 days in the absence of bFGF. Neuronal maturation was stimulated by growing cells for 3 days in Neurobasal media with the B-27 supplement, neurotrophin 3 (NT3), and brain-derived neurotrophic factor (BDNF). Using voltage-clamp recording (Supplemental Experimental Procedures), we showed that this condition promotes excitable currents in 87% of the cells with neuronal morphology without the need for exogenous astrocytes or serum (Figure S1 and Table S1). These conditions that support functional neuronal differentiation are used as control conditions throughout this work.

To image the specification of progenitor cell types, we developed a culture chamber that controls media and gas exchange over the microscope stage, emulating the environment in a tissue-culture incubator (Figure S2 and Supplemental Experimental Procedures; U.S. Patent Number 7,091,035). Imaging every 2 minutes with a 40× oil immersion objective gave sufficient time and space resolution for complete lineage analysis. In total, this work is based upon the complete lineages from 326 founder cells. Manual tracking of these founders produced lineages for a total of 7269 cells after expansion and differentiation.

Fate Specification Occurs Early

Figure 1A shows single frames taken from 4,860 images (Movie S1). The low frequency of cell loss due to migration out of the visual field was achieved by restricted growth areas (Figure S3; U.S. Patent Number 7,276,367). Epifluorescence from conjugated fibronectin shows this area in the first panel that is outlined at day 4. This area contains 4 cells at the beginning of the recording (12 hr after plating) and 43 cells 7 days later when cell identity was established using immunoreactivity and morphology (last panel in Figure 1A). Cells with unambiguous oligodendrocytic morphology that die before fixation are labeled as oligodendrocytes. The lineage dendrogram in Figure 1B is derived from analysis of Movie S1.

By marking the terminal leaves on the lineage tree with colors that represent discrete fates, one observes a clustering of common fate among closely related cells (Figure 1B). The observation that terminal cells derived from a common ancestor share the same fate could reflect early specification of the ancestor or a random series of coincident events. To address these competing hypotheses, we developed a statistical hypothesis testing procedure that uses terminal cell fates and mitosis times to calculate the probability that the distribution of same-fate siblings is random or nonrandom throughout the entire period of culture. Applying this test to the last time point in the experiment, we found that the occurrence of same-fate siblings is not random. Testing earlier time points, we identified the time at which the average probability of same-fate siblings becomes nonrandom ($p > 0.05$). This point is marked with an asterisk in Figure 1B (see Supplemental Experimental Procedures for details). This early specification of fate was validated by multiple approaches described below.

Based on this statistical evidence, we retrospectively labeled cells as specified if they give rise to only one cell type. Parent cells are labeled with the fate of their daughters if both daughter cells share the same fate (Figure 1C). If siblings do not share the same fate, then the parent cell is labeled as unspecified. Lost and unstained cells are treated as alternative known fates. If two siblings die, then the parent is specified as a dying cell. However, if a single daughter cell dies, then the parent is specified by the fate of the surviving daughter. This decision is justified because the majority of dying cells in control lineages occur in later generations when sibling cells normally share the same fate (shown later in Figure 4A). Figure 1D is derived from Figure 1B using retrospective annotation. A consequence of annotating lineages with this rule is that the point of specification can be identified by the transition from black to color (Figure 1D). This point correlates well with the time when sibling cell fates become statistically nonrandom (asterisk in Figure 1D).

In Figure 1D, Cell 1 is annotated as a specified oligodendroglial progenitor since it produces four generations of cells which, beside two early deaths, are all identified as oligodendrocytes. Cells 2 and 3 each produce three cell types, and cell 4 produces two terminal cell types within three generations. This typical example of four cells from one experiment demonstrates the high degree of heterogeneity in CNS stem cell cultures. The emergence of specified (colored) cells and their positions are depicted in Figure 1E. The time-lapse representation in Movie S2 shows again the spatial and temporal appearance of specified cells. The control group contains lineages from 35 founders that produced 897 terminal cells. The fate distribution was 34% neurons, 28% astrocytes, and 19% oligodendrocytes. Five percent did not express detectable levels of lineage specific antigens, 6% were lost, and 8% died.

If cells are classified as unspecified or specified, three discrete temporal phases of cell division emerge (Figure S4A). At early times, unspecified cells divide to produce more unspecified cells. Later, divisions occur where one daughter is specified and the other is not. Subsequently, the culture is dominated by the expansion of specified cells. By plotting the cumulative number of cells of each fate through generations, the onset of specification of the neuronal, astroglial, and oligodendroglial lineages is seen to be early and synchronous (Figure S4B). Note that the cells were maintained in the presence of bFGF up to generation four, demonstrating that specification to the unipotent state occurs while cells are dividing in the presence of mitogen. Day 2 in Figure S4C is equivalent to generation 4 in Figure S4B. Fate

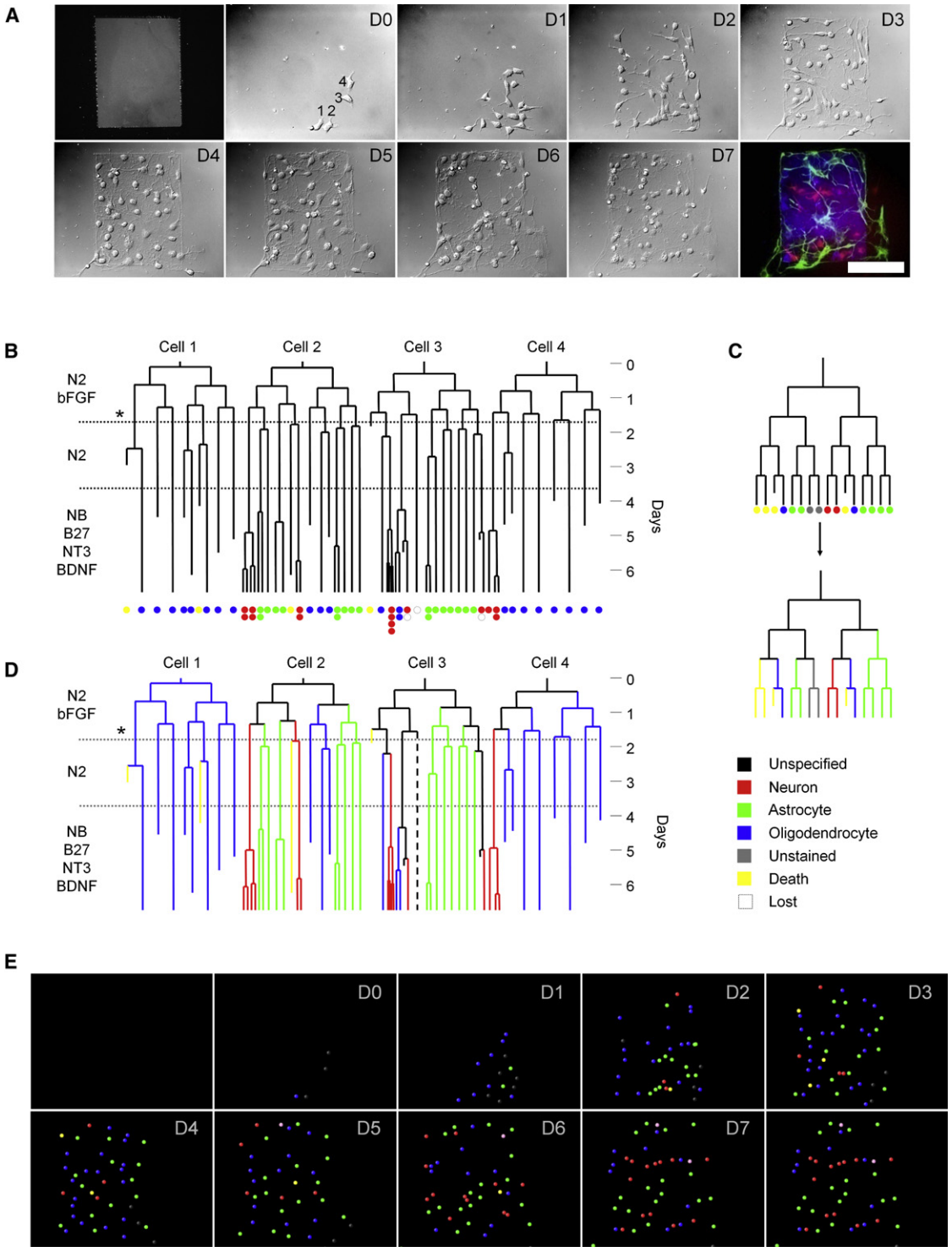

Figure 1. Lineage Analysis of a Time-Lapse Recording from a Single Area Demonstrates Early Fate Specification in Neural Lineages

(A) Time-lapse images of expanding and differentiating rat neural progenitors. D0–D7 reflect days after first image. Numbers in D0 refer to cells in (B) and (D). Dotted outline in D4 represents the border of the permissive growth area. Scale bar, 100 μm. Still images are taken from Movie S1. Immunofluorescence shows neurons in red (TUJ1), astrocytes in green (GFAP), and oligodendrocytes in blue (CNPase).

(B) Lineage dendrogram of time-lapse data. Media changes are indicated on the left (N2, DMEM/F12 with N2 supplement; bFGF, basic fibroblast growth factor; NB, NeuroBasal; NT3, Neurotrophin 3; BDNF, brain-derived neurotrophic factor). Colored circles represent final fates corresponding to the colors in (A).

(C) Schematic diagram of rules used to transform lineage dendrograms with final fates into lineage fate maps showing early points of specification.

specification begins by generation 3 to 4 (day 2). Most cells express fate-specific epitopes only after several days of differentiation (day 5 for neurons and day 6 for astrocytes and oligodendrocytes, Figure S4C). Thus, the time of specification precedes the appearance of fate-specific epitopes by 2 to 3 days.

A Rapid Potency Change in Proliferating Cells

To assess the potency of unspecified cells, each was assigned a potency reflecting the terminal descendants it generates (Figure 2A). This representation is shown in Figure 2A for the same lineage as in Figure 1. A summary of all this control data demonstrates that at the beginning of imaging, 57% of the cells are tripotent (black diamonds), 31% are bipotent (open circles), and 11% are already unipotent (open triangles; Figure 2B). Within three generations, the proportion of tripotent cells falls to less than 10%. These data show, in a statistically robust manner, that rapid loss of tripotency is concurrent with a transient increase in the bipotent population. Later, a stable increase in the unipotent population dominates. Withdrawal of the mitogen bFGF is thought to induce fate choice (Cattaneo and McKay, 1990). However, at this point (generation 4), 80% of the cells are already specified into a single fate. These data demonstrate that cell-fate specification occurs in dividing cells in the presence of bFGF.

To confirm the conclusion that cultured CNS stem cells are specified in the presence of bFGF, we cultured cells in the presence of bFGF for an additional 2 days. We achieved the additional days of culture by reducing cell density through random laser ablation at the normal time of bFGF withdrawal (Figure 2C; Figure S5; Supplemental Experimental Procedures). According to control lineage data at the time of bFGF withdrawal (control generation 3), the population is estimated to have 6% tripotent cells, 49% bipotent cells, and 42% unipotent cells. Lineages for 43 founder cells after ablation show that the surviving cells were 5% tripotent, 44% bipotent, and 51% unipotent at the first time point (Figure 2C). The potency distribution immediately after ablation almost perfectly overlaps with the potency distribution at the relevant point in the control population in Figure 2B, despite continued cell division in the ablation experiment in the presence of bFGF. These data demonstrate that cells are specified with the same kinetics whether cultured for 2 1/2 days or 4 1/2 days in the presence of bFGF.

The apparent potency of a cell is related to the number of progeny produced by the cell; a true tripotent cell that divides only once to produce two specified cells would, at most, appear as a bipotent cell. If apparent bipotent cells were given the opportunity to make additional cell divisions in the presence of bFGF, their actual potency might be revealed. The laser ablation results demonstrate that apparent potency is not a consequence of limited cell divisions and that cell-fate specification occurs in the presence of bFGF.

Resetting Potency

Previous work from our lab demonstrated that most neural progenitors remain multipotent through passage (Johe et al., 1996). Lineages established after the third passage show that after passage 3, 42% of the population is tripotent (Figure 2D). Although the kinetics of fate restriction differ slightly in passage 3 compared to passage 1, the two populations resemble one another both in proportion and progression of fate restriction.

The frequency of tripotent cells is less than 2% after four generations in the presence of bFGF (Figure 2B). As cells are normally passaged every 2 to 3 days (equivalent to 4–6 generations), the size of the tripotent population is expected to be near zero at this time. The high frequency of tripotent cells at passage 3 (Figure 2D) could be a consequence of selection for multipotent rather than specified cells through passage. To determine the feasibility of the selection hypothesis, we calculated passage efficiency by directly counting cells before, during, and 2 hr after passage from passage 1 through passage 3. The plating efficiency at each passage is 0.8. If there was strong selection in favor of the tripotent cell at passage, then the maximum proportion of tripotent cells after the third passage would be $2\% \times 1/0.8 = 2.5\%$. After passage three, the tripotent population is 42%, showing that selection at passage cannot explain the persistence of the multipotent state through time. These data suggest that passage resets cells to a more primitive state.

Nonrandom Exit from the Tripotent State

To more precisely define changes as multipotent cells become specified, we measured the types of transitions between parent cells and their progeny. Using results from 20 tripotent founder cells and eight bipotent founder cells, we tabulated the number of events generating new tripotent, bipotent, and unipotent cells at each generation in 50 tripotent cells, 174 bipotent cells, and 244 unipotent cells represented across seven generations (Figure 2E). Self-renewal of a tripotent cell is common early but diminishes rapidly through generation. After the first division, the most common product of a tripotent cell is a bipotent cell. Likewise, bipotent cells show a short phase of self renewal and rapidly switch to the production of unipotent cells. This network of changing states shows that tripotent cells almost always become specified through bipotent intermediates. Statistical analysis of observed and expected numbers of tripotent, bipotent, and unipotent cells supports the nonrandom transition from tripotent to bipotent and bipotent to unipotent cell types (Figure S6).

The expression of CD15 has been proposed as a tool for prospective isolation of stem cells from the adult and fetal brain (Capela and Temple, 2002, 2006). CD15 is coexpressed with CD133, and both epitopes have been used to perform fluorescence-activated cell sorting (FACS) isolation of multipotent neural progenitors (Capela and Temple, 2002, 2006; Panchision et al., 2007; Uchida et al., 2000). We found a weak correlation between CD15 expression and loss of potency at the population level; however, no correlation was seen between CD15 expression and founder cell potency or the number of progeny derived from individual cells (Supplemental Data and Figure S7). The lack of correlation between early CD15 expression and potency or proliferative capacity in single lineages prompts cautious interpretation of the expression of surface epitopes without a precise lineage analysis.

CNTF and Astrocytic Fate Choice

To determine when fate choice can be modified by exogenous signals, cells were exposed to CNTF. This ligand has been widely

(D) Transformation of (B) using rules in (C). Asterisk indicates the calculated average time of nonrandomness for this lineage. (E) Ball representation of cell position and cell fate from (A). Still images are taken from Movie S2.

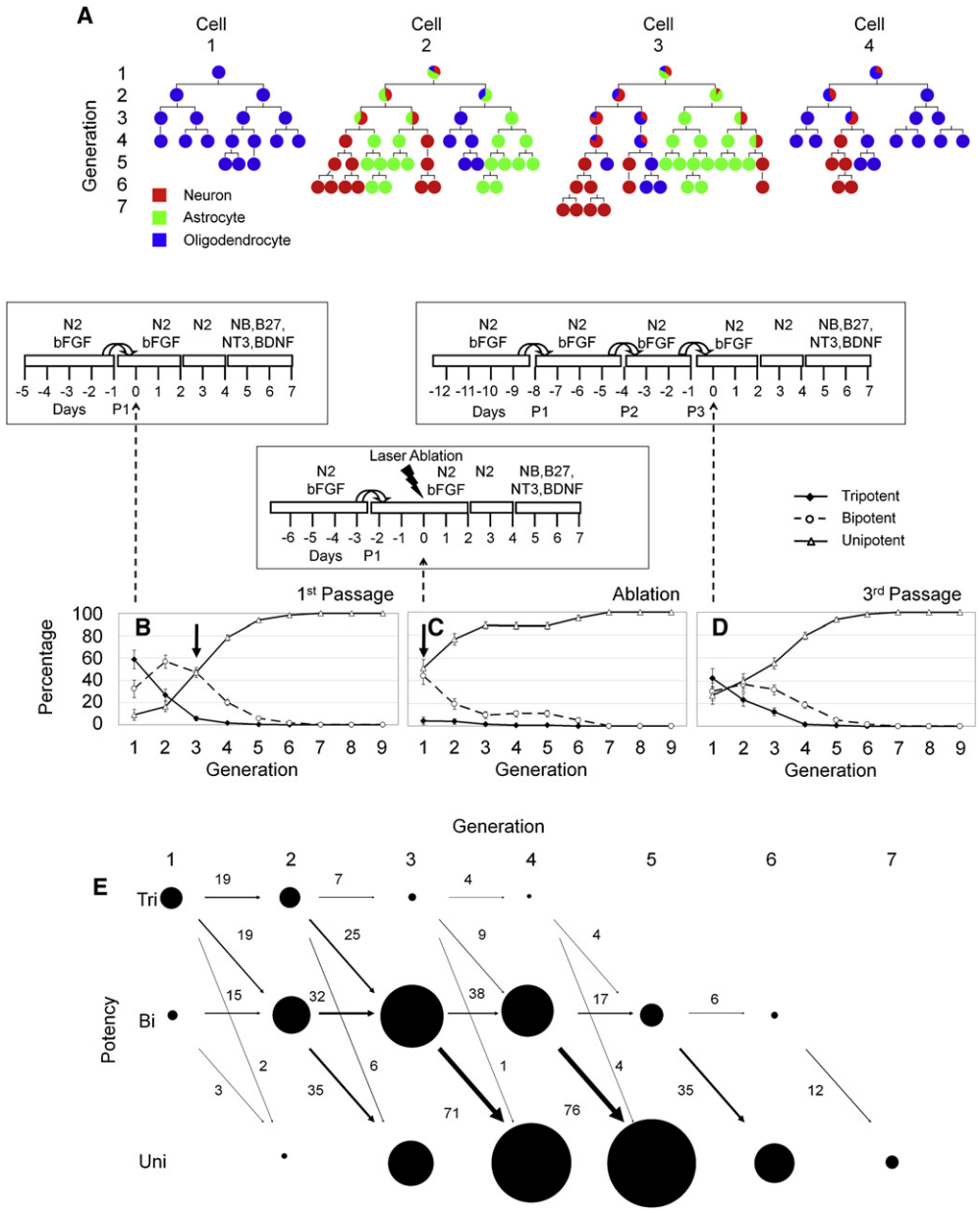

Figure 2. Multipotency Is Rapidly Lost in the Presence of bFGF but Is Regained by Passage

(A) Each pie chart represents an individual cell from the lineage in Figure 1. Color distribution inside each cell represents its final fate distribution. Lost and dead cells are excluded from the image for clarity. Siblings of lost or dead cells are indicated by a straight vertical line such as in the leftmost lineage in Cell 1.

(B–D) Percentage of new cells produced at each generation. Tripotent, black diamonds; bipotent, open circles; specified, open triangles. Boxes above indicate the experimental design. (B) First passage (n = 35 founder cells). Arrow denotes the point of laser ablation for the culture in (C). (C) Fate distribution after laser ablation at generation 3, first passage. Note the similar cell-class distribution between the first time point after ablation and the third generation in (B), (n = 43 founder cells). (D) Resetting of cell-fate potency after passage 3. Fate distribution of new cells produced at each generation after the third passage (n = 33 founder cells).

(E) Total numbers of tripotent and bipotent founders and their descendants from all control experiments are represented as circles, where the dimensions are proportional to their true abundance at each generation (generations shown on the x axis and potency shown on the y axis). Transitions in potency from parent to daughter are represented by arrows. The width of each arrow represents the number of each type of transition measured in the lineage. The number reflects the exact number of each transition across each generation.

The error bars in (B), (C), and (D) reflect the mean percentage ± SEM.

used to study astrocytic fate choice and differentiation (Barnabe-Heider et al., 2005; Bonni et al., 1997; Johe et al., 1996; Rajan and McKay, 1998; Song and Ghosh, 2004). Figure 3A outlines the experimental design for CNTF treatment. To determine the change in plasticity through time, control media was supplemented continuously with CNTF either 3 hr before ($CNTF^{-3}$;

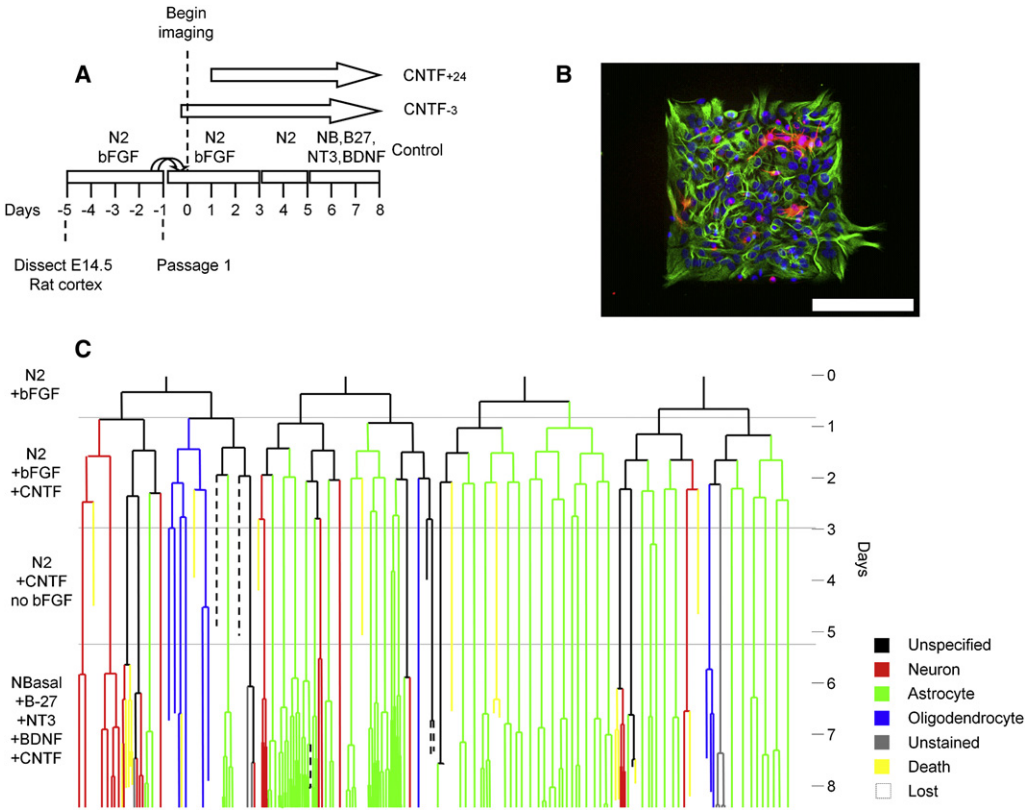

Figure 3. CNTF Biases Multipotent Neural Progenitors toward the Astrocytic Fate through Early Instruction and Late Expansion of Astrocytic Progenitors

(A) Experimental design of CNTF treatment.

(B) Immunofluorescent image of last frame of movie in Movie S3. Neurons are shown in red (TUJ1), astrocytes in green (GFAP), and nuclei are stained with DAPI.

(C) Lineage fate map of Movie S3. Note the late astrocytic divisions in (C).

32 founder cells) or 24 hr after initiating imaging ($CNTF^{+24}$; 43 founder cells). Exposure to CNTF promotes the production of astrocytes that express high levels of glial fibrillary acidic protein (GFAP) (Figure 3B). This endpoint image demonstrates that the field is dominated by GFAP-positive astrocytes but also contains several neurons. Figure 3C shows a representative lineage of rat CNS stem cells treated continuously with CNTF. The most striking change in the CNTF-treated lineage is seen in the late expansion of specified astrocytes (compare Figures 3C and 1D).

To quantify the response of different cell populations to CNTF, we calculated the number of tripotent and type of bipotent and unipotent cells at each generation with and without CNTF treatment. All values shown were normalized to the 35 founder cells lineaged in the control population. CNTF treatment increased the number of dying progenitors (Figure 4A). In control cultures, every neuron and astrocyte was unambiguously classified by marker expression and morphology. In $CNTF^{+24}$ cultures, low numbers of cells coexpressed both astrocytic and neuronal markers with an ambiguous morphology. In $CNTF^{-3}$ treated cells, there was a significant increase in the number of double-stained cells accounting for 3% of the total cells from $CNTF^{-3}$ lineages (Figure 4B). This new cell population was scored as a separate fate.

Lineage analysis showed that the tripotent population was slightly reduced in $CNTF^{+24}$ and significantly reduced in $CNTF^{-3}$ lineages (Figure 4C). This might be expected from the larger number of tripotent cells available to respond at −3 hr. Notice that a significant difference from the control occurs in the $CNTF^{+24}$ lineage only after generation 3, consistent with the later addition of CNTF. These data show that CNTF treatment clearly reduces the number of tripotent cells (Figure 4C). The number of NA and AO cells was also reduced, but there was a lesser effect on the NO populations (Figures 4D, 4E, and 4F). The analysis of unipotent cell types shows reduced numbers of neurons and oligodendrocytes (Figures 4G and 4H). In contrast, the production of astrocytes was enhanced (Figure 4I).

One explanation for the reduced NAO, NA, and AO populations and increase in the astrocytic population would be that tripotent cells are directly specified as astrocytes, bypassing the normal bipotent intermediates. Increased astrocytic output from NA and AO cells might provide an alternative explanation for increased astrocyte numbers. To resolve these possibilities, a database was constructed that reports every transition from tri-, bi-, and unipotent parent to tri-, bi-, and unipotent daughter cell at each generation. These data were used to define the frequency of each possible cell-fate transition. The number of transitions from one generation to the next is plotted and, as we are comparing different experiments, the data were normalized to the number of cells in the control. The $CNTF^{+24}$ and $CNTF^{-3}$

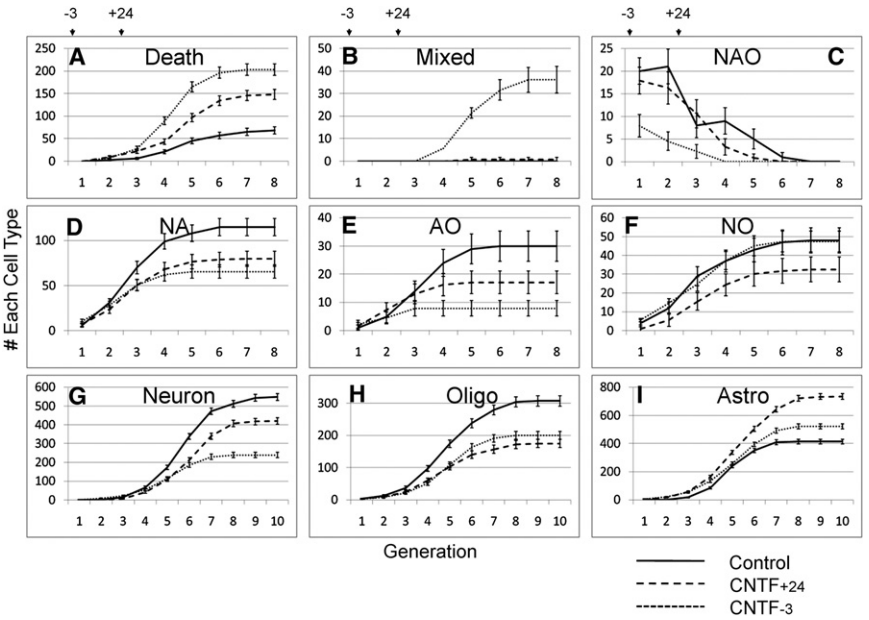

Figure 4. Population Dynamics during CNTF Treatment Reveals Sensitive Target Cells and Sensitive Target Periods

(A–I) Cell counts of discrete cell types in each generation normalized to the total founding number of cells in the control. CNTF added 3 hr before (−3) or 24 hr after (+24) imaging. (A) Cumulative number of dying and (B) mixed cells. (C) Normalized number of tripotent cells in each generation. (D–F) Cumulative number of bipotent cells; (G–I) Cumulative number of unipotent cells; variance is calculated as standard error for a binomial distribution. Arrowheads above (A), (B), and (C) indicate the time of CNTF addition. N, neuron; A, astrocyte; O, oligodendrocyte; NAO, Tripotent; NA, NO, and AO, bipotent; D death; M, mixed.

treatments reduce the number of transitions from NAO to NA and AO (the bipotent cells that give rise to astrocytes) (Figures 5A and 5B). In contrast, the transition from NAO parent to NO daughter was unaffected by either CNTF treatment (Figure 5C). The production of astrocytes from NA and AO cells was reduced by CNTF treatment (Figure 5D). Therefore, the increased numbers of astrocytes must be caused by events that occur prior to establishing the bipotent state.

The same analysis demonstrates that NAO to A transitions are significantly increased by CNTF treatment (Figure 5E). The late proliferative effect of CNTF contributes most of the increased numbers of astrocytes seen at the end of the differentiation period (Figure 5F). These data summarized in Figure 5G show that the increase in astrocytes induced by CNTF is caused by two distinct cellular mechanisms: an early instructive and a later selective effect.

The early positive proastrocytic effect on tripotent NAO cells is a remarkable feature of these data. The probability of transitions from the NAO to bipotent states was modified in an interesting way by CNTF treatment. The number of NO progeny was unaffected, but fewer NA and AO cells were generated when increased numbers of A cells were produced. In the CNTF-treated condition, the probability that bipotent cells produce astrocytes was also altered. Surprisingly, the probability of astrocyte production from bipotent cells was reduced. These data show that CNTF exerts both positive and negative instructive effects on astrocytic fates. There is a strong positive effect on the tripotent, and a negative effect on bipotent, cells.

Induction of GFAP Expression

The assignment of fate in time-lapse lineage dendrograms is based upon terminal immunoreactivity and retrospective analysis. A specific intermediate filament protein, glial fibrillary acidic protein (GFAP), is expressed in astrocytes and in precursor cells in the adult brain (Doetsch et al., 1999). Two approaches were used to relate the lineage data to this widely used molecular marker of the astrocytic state. First, we measured the induction of GFAP expression by CNTF at shorter times to increase confidence in the retrospective fate assignment. Second, a regulatory element from the GFAP gene was used to measure promoter activity in real time in all cells throughout a lineage analysis.

GFAP expression was assessed in cell populations fixed each day after continuous CNTF treatment (Figure S8A). GFAP expression is detected rapidly in the $CNTF^{+24}$ condition, and complete lineages were generated for the 36 hr following CNTF treatment (Figure S8B). Astrocytic fate was assigned to GFAP-expressing cells, but other fates were not assessed due to lack of antigen expression at this early time point. As seen in the previous long-term studies, GFAP-expressing cells tend to have sisters that also express GFAP. Retrospective analysis reveals that the number of specified astrocytic progenitor cells is nearly identical in the 36 hr and 8 day experiments (Figure S8C). The short-term analysis of GFAP expression supports our previous conclusion of early fate specification.

Fluorescence from a GFAP-GFP reporter in individual living cells was used to examine early fate specification more precisely in the astrocytic lineage. Neural stem cells were infected with a lentivirus encoding the mouse GFAP promoter driving GFP. The viral transgene provides robust GFP signal only in cells that also express the endogenous GFAP protein (Figure S9). Due to a destabilizing sequence in the GFP reporter, it is possible to measure the short-term activity of the promoter. To assess the dynamic activity of this reporter at different phases of lineage development, we took advantage of the continuous perfusion and easy access built into the chamber design. These features allowed pulse-chase experiments with brief exposure to CNTF at 0.5 days, 1.8 days, and 3.5 days during time-lapse imaging. The pulse was followed by a chase where the medium in the chamber was completely changed. These times were chosen to probe early, middle, and late phases of lineage specification. Fluorescence images to measure GFP expression were acquired every 12 hr for 3 days, then daily for the balance of the experiment. These fluorescence images were interleaved at the appropriate place in the DIC image stack (Movie S4). This allowed the construction of fate maps where individual cells were annotated with fluorescence signals throughout their lineage.

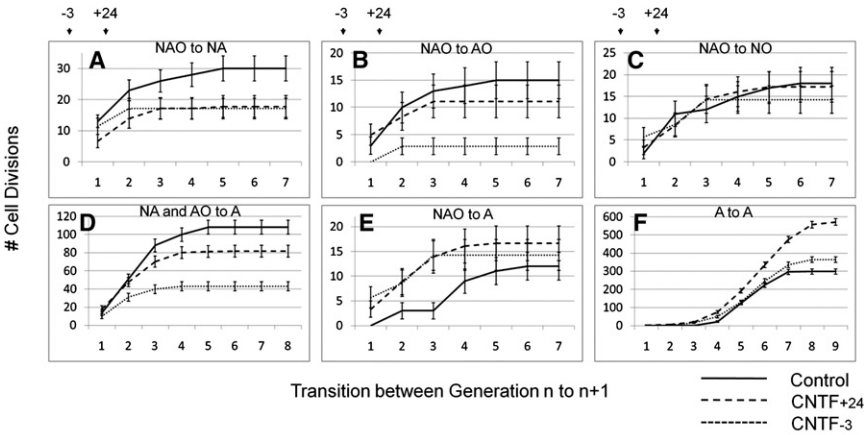

Figure 5. CNTF Biases Normal Parent to Daughter Transitions in Potency toward Precocious Production of Astrocytes

(A–C) Tripotent parent to bipotent daughter transitions.

(D–F) All sources of astrocytes. (D) Bipotent parent directly to astrocytic daughter (E) Tripotent parent directly to astrocytic daughter. (F) Specified astrocytic progenitor to astrocyte. Transition 1 occurs between generation 1 and 2. (G) Schematic model of CNTF action on CNS stem cell cultures. CNTF promotes astrogliogenesis by direct specification of tripotent cells into the astrocytic fate and later selective expansion of specified astrocytes. Dotted lines and reduced font size indicate fewer events. Variance is calculated as standard error for a binomial distribution.

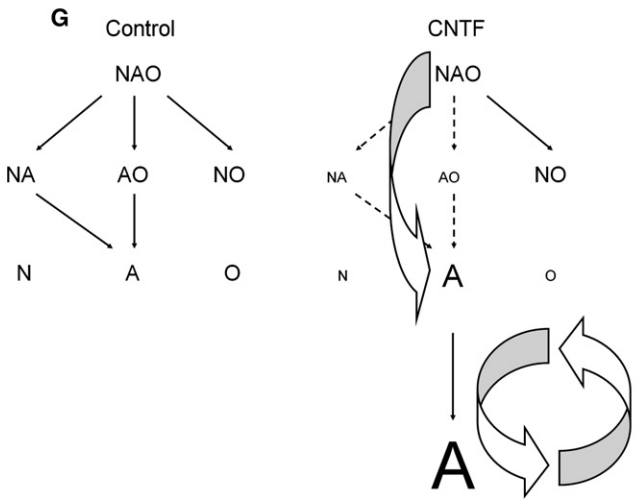

The retrospective lineage analysis shows that astrocytic fate specification occurred on average on day 1.3 (±0.6, n = 32; marked by black arrow in Figure 6A). The lineage dendrogram and associated micrographs shown in Figure 6A demonstrate that the change in fluorescence through time in specified astrocytes and other fates is clearly different by day 3.5. At day 2.5, other fates can also express the reporter. However, this weak expression is only transient and contrasts with the continued increase in promoter activity seen in specified astrocytes. In the quantitative summary of changes in promoter activity through time, a clear increase in signal is first seen on day 2.5 (Figure 6B). At this time, transcriptional activation of the reporter occurred in both astrocytic and nonastrocytic cells but was only sustained in specified astrocytes. These results unambiguously validate the early differences between lineages predicted by the long-term retrospective analysis. The difference between the time when astrocytic fates are seen using lineage analysis and GFAP expression points to the importance of further studies on the early events that generate distinct cell fates.

DISCUSSION

Stem cells are defined by the ability to self renew and give rise to specified cell types. In vitro cultures of neural stem cells can recapitulate the expansion, specification, and maturation of each of the major cell types in the mammalian CNS. For most therapeutic applications, cells must be expanded in vitro before grafting. Thus, the detailed characterization of cultured CNS stem cells merits attention from the research community as well as the cell-based therapeutic community. The limitation of in vitro analysis is that results achieved in vitro cannot be directly extrapolated to the environment in vivo. For long-term lineage analysis, the only reasonably tractable system is a dissociated culture system such as the one employed here. We focused our studies on the E14.5 rat cerebral cortex because this particular developmental stage and brain region provides reproducible access to the neuronal, astrocytic, and oligodendroglial fates. One might expect that cells from earlier developmental stages would consist of a more substantial multipotent self-renewing population and older cells would be more specified.

Cell type is typically defined by morphology, behavior, or the expression of specific epitopes, yet these are often far downstream from the decision points in cell-fate specification. We define the point of cell-type specification as the mitosis that produces only one cell type. Significant evidence supports the asymmetric localization of cell-fate determinants prior to mitosis (Chenn and McConnell, 1995; Lu et al., 2000; Sun et al., 2005), but mitosis is required to segregate discrete fates into daughter cells. We, therefore, accept mitosis as the earliest point of cell-fate specification and label lineage dendrograms using this approach. Our ablation study demonstrates that our determination of potency in vitro is accurate and that the tripotent population has almost disappeared by generation 3 to 4. These processes all occur in mitotic populations in the presence of bFGF. Therefore, there is no correlation between withdrawal from the cell-cycle and cell-type specification. The rat cerebral cortex at E14.5 is comprised largely of a mitotic population that does not express epitopes of specified cells. Significant changes in

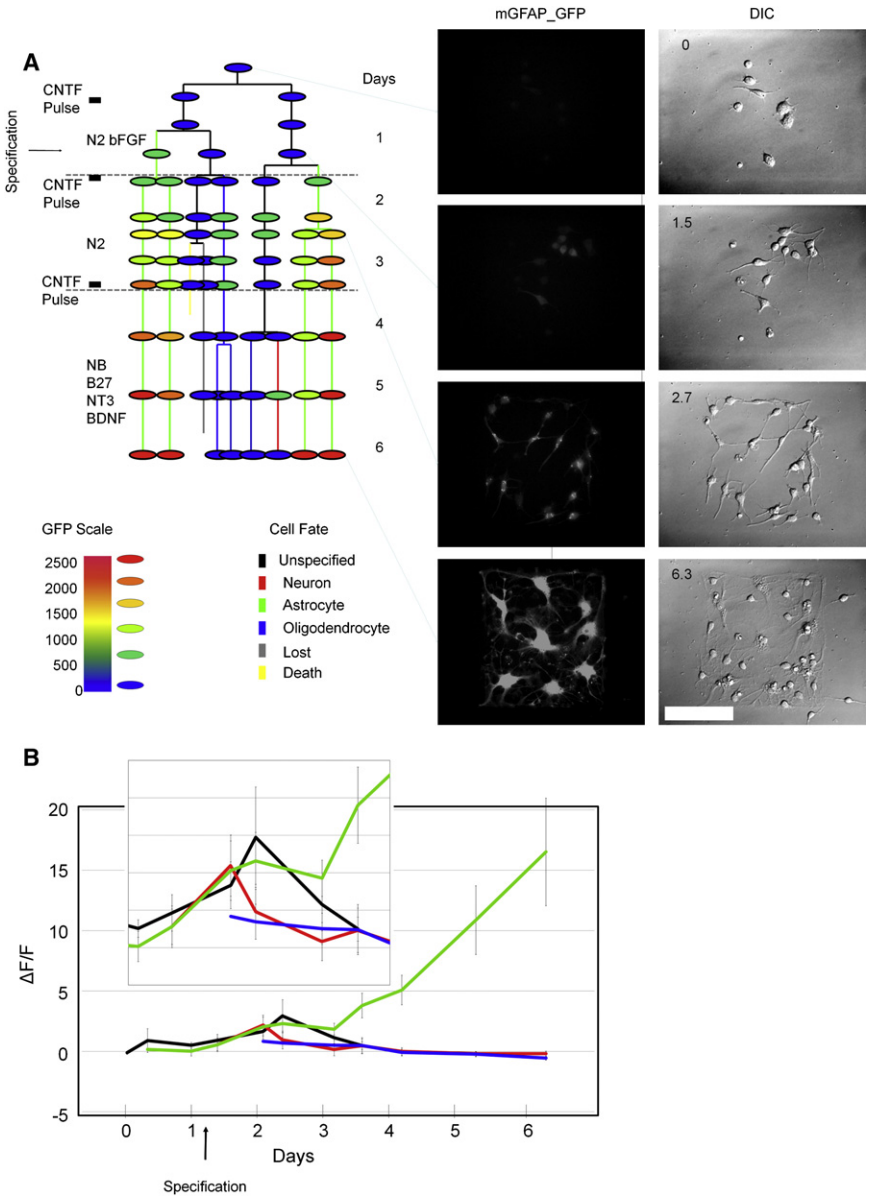

Figure 6. GFAP Reporter Expression in Neural Stem Cell Lineages Validates Early Astrocytic Fate Specification

(A) Lineage fate map from a single infected founder cell. The vertical colored lines represent fate. The colored ovals indicate GFP expression level at each point of fluorescence imaging. The GFP scale represents mean fluorescence, in arbitrary units, as discrete colors. Example fluorescence micrographs and corresponding DIC micrographs demonstrate the background-subtracted signal for each cell. Scale bar, 100 μm. Media conditions and CNTF pulse chase are shown to the left (black boxes represent the duration of CNTF pulse).

(B) ΔF/F at the indicated time points. The inset magnifies the low values centered at day 2.5. Error bars reflect SEM.

cell-cycle regulation occur during midgestation corticogenesis (Caviness et al., 1995; Fasano et al., 2007). It is possible that the kinetics of fate specification we observe is a consequence of the specific developmental stage or of the specific in vitro system we used. However, it is also possible that the mitotic populations observed in vivo are actually proliferating specified cell populations.

The opposition between self-renewal and differentiation mechanisms in a single cell has been explained by symmetric and asymmetric cell division (Morrison and Kimble, 2006; Noctor et al., 2004). A reiterative asymmetric neurogenic program has been identified in acutely isolated mouse neural stem cells before passage (Qian et al., 2000). In contrast, the goal of our work was to understand the lineage mechanisms in cells that are expanding. In our system, the stem cell state was not maintained by asymmetric self-renewal but through resetting of more specified cells to a higher level of potency at passage (see ablation discussion above). There is significant interest in the mechanism of reprogramming somatic cells to a pluripotent state after viral transduction (Takahashi and Yamanaka, 2006). It has also been demonstrated that it is harder to reprogram fully differentiated B cells in the hematopoietic system (Hanna et al., 2008). Resetting specified neural stem cells to a higher state of potency is a robust and simple procedure that reveals the plasticity of the specified state. The fact that these cells are able to be reset demonstrates that their fate was specified and not committed. This simple system provides new tools in the investigation of the epigenetic mechanisms that maintain and restrict stem cell potency.

Our analyses demonstrate that CNS stem cells cultured from the midgestation cortex are heterogeneous in developmental potency. We examined the plasticity of this heterogeneous population using an exogenous ligand, CNTF. CNTF acts instructively at early times to generate increased numbers of astrocytes, bypassing the normal NA and AO bipotent intermediates. At late times, astrocytic progenitors show increased response to CNTF measured by changes in the activity of the GFAP promoter and enhanced proliferation. The endogenous GFAP gene expression and a GFAP-reporter construct confirm that CNTF-responsive astrocyte progenitors can be uniquely identified 2 days after fate specification (Figure 6). Considering GFAP is a downstream consequence of astrocytic fate specification and GFP fluorescence requires expression and maturation, we expect a delay in reporter expression after fate specification. GFAP expression is thought to define multipotent neural precursors in the adult brain (Doetsch et al., 1999). In vitro experiments show that a combination of STAT3 and SMAD signaling is required for GFAP induction in neural stem cells (Fukuda et al., 2007; Nakashima et al., 1999). Complete lineage analysis using GFAP_GFP now defines an early narrow time window for

astrocytic fate specification in cultured neural stem cell populations. The lack of correlation between the stem cell state and CD15 expression indicates that more robust markers of unspecified cell types would be beneficial. Lineage analysis will play an important role in identifying and validating such markers. Our analysis demonstrated that instructive and selective mechanisms can act on different elements of a single stem cell clone. Further development of this approach will enable the identification of relevant intermediates and define their specific contributions to the production of heterogeneous populations such as tissues and organ systems.

EXPERIMENTAL PROCEDURES

Cell Culture

Embryonic day 14.5 embryos were extracted from pregnant Sprague-Dawley rats according to the NINDS guidelines. Cerebral vesicles were isolated without enzymatic digestion as previously described (Johe et al., 1996) and plated at 20,000 cells/cm^2 in poly-L-ornithine /fibronectin-coated 10 cm tissue culture plates (1.0 × 10^6 cells) and grown for 4 days in DMEM/F12 (MediaTech) with N2 supplement using human apo-transferrin (Sigma), human bFGF (R&D Systems, 10 ng/ml), and insulin (Sigma, 25 ng/ml). bFGF was added daily with complete media replacement every second day. To passage cultures, cells were gently passaged in HBSS (GIBCO 14185-042) with added HEPES (3.9 g/l) pH 7.1 and plated at 10,000 cells/cm^2 onto 24.5 mm coverslips (1.0 size, Carolina Biological) coated as described below.

Long-Term Imaging of Migratory Cells

Restricting cells to the field of view was accomplished by creating 300 μm rectangular islands of extracellular matrix with an etching device (Figure S3). Restricted growth areas are created by coating sterile 25 mm round coverslips (Assistent, Karl Hecht KG) with 500 mg/ml poly-L-ornithine (Sigma), then Bovine fibronectin 10 μg/ml (R&D Systems) previously dialyzed against 1000 volumes of PBS. Fibronectin is indirectly visualized by fluorescence from Alexa 555-conjugated fibronectin (Monoclonal Antibody Labeling Kit, Invitrogen). Coverslips are seeded with CNS stem cells then etched to create islands (see Figure S3 for diagrams and discussion).

Live-Cell Chamber

The system is composed of two chambers, (A) a novel gas-tight wet/dry chamber that we designed to regulate media and gas composition (U.S. Patent number for live-cell chamber: 7,091,035) and (B) a custom opaque light-tight outer chamber that allows precise temperature regulation (Precision Plastics, Beltsville, MD). Using the gas-tight chamber, we maintained a 5% CO_2, 5% O_2 environment and performed complete media changes while continuously imaging. Temperature was regulated (37°C ± 0.1°C) using an AirTherm (WPI). Between media changes, media was perfused at a rate of 30 μl per hour using 25 ml gas-tight syringes (Hamilton) and a syringe pump (Harvard Apparatus). Stainless steel tubes connect the syringe to the growth chamber (see Figure S2 for arrangement).

Imaging

Cells were imaged using a Zeiss Axiovert 135TV microscope with a 40×, 1.3 NA oil-immersion objective. DIC images from single restricted growth areas were captured with an Orca ER (Hamamatsu) CCD camera every 2 min. To image multiple areas from one experiment, we used a computer-controlled motorized stage (Ludl Mac5000) with a linear encoder. Metamorph software (Universal Imaging) was used to control all components. To minimize phototoxicity, 15 ms exposure times were achieved using a shutter (UniBlitz).

Immunostaining

Cells were fixed with 4% paraformaldehyde and then stained for lineage-specific antigens without removing the live-cell chamber from the microscope stage. Cells were blocked in 10% normal goat serum with 0.1% Triton X-100, then labeled with mouse anti-CNPase IgG$_1$ (Chemicon), mouse anti-BIII-tubulin IgG$_{2A}$ (TUJ1, R&D Systems), rabbit polyclonal anti-Glial Fibrillary Acidic Protein (DAKO), and DAPI (Sigma). For surface staining with SSEA-1 (MC-480 from Developmental Studies Hybridoma Bank), Triton was omitted. Secondary antibodies include Alexa 568-labeled goat anti-mouse IgG1 (Invitrogen), Alexa 488-labeled goat anti-mouse IgG$_{2A}$ (Invitrogen), and Cy5-labeled goat anti-rabbit polyclonal (Jackson Immunoresearch). For live-cell staining with CD15-FITC (Becton Dickinson), cells were incubated with antibody (8 μg/ml) for 15 min without blocking and then washed three times with media before fluorescent images were acquired. To quantify fluorescence in CD15-FITC stained samples, we used ImageJ (NIH) to define regions of interest within the soma of each cell. Reported values are average fluorescence minus average background from adjacent areas.

Lineage Analysis

Full-length recordings were assembled into stacks using Metamorph, AVIEdit, and ImageJ. TIFF stacks of time-lapse data were stabilized using the ImageJ plugin Image Stabilizer. Contrast was enhanced using the Shadow Illuminator plugin (Intrigue Technologies) to Photoshop CS (Adobe). Lineages were manually generated and annotated for terminal fates and mitosis times using SIMI°BioCell (Schnabel et al., 1997). Using Lineage Analyzer (Custom programmed by EYE Biomachines for this application) and Microsoft Excel, we calculated cell-fate potency based upon cell output: tripotent cells produce at least one neuron, one astrocyte, and one oligodendrocyte. Bipotent cells produce two fates, and unipotent cells produce only one. Lost, dying, and unstained cells were excluded from summary calculations. The rationale for excluding dead and lost cells (each contributing 6% and 8%, respectively, of total terminal fates) is that most lost and dying cells are found in late generations after cell-type specification has already been established. Therefore, it is likely that dying cells and surviving siblings would share the same fate, and therefore, not alter parent cell fates. The rationale for excluding unstained cells (5% of total) is that a large proportion of these unstained cells appear like young specified progenitors that have simply not expressed terminal markers. These cells, when stained with anti-nestin antibodies, are nonreactive (data not shown), suggesting that they are not persistent stem cells.

Lentiviral GFAP_GFP Reporter Analysis

Lentivirus encoding the 1.7 Kb mouse GFAP promoter and copGFP was purchased from System Biosciences Inc. A multiplicity of 16 particles per cell resulted in a productive infection in roughly half the cells. Unlike other experiments, here we used rat neural stem cells that were frozen at the first passage. Frozen cells were plated and infected with virus immediately in N2 + bFGF for 12 hr. Forty-eight hours later, cells were passaged onto glass coverslips for long-term culture and imaging. Epifluorescence images were captured each 12 hr until day 3½ and then daily afterward using the same acquisition parameters—100 ms exposure with a neutral density filter that reduces the exposure of cells to fluorescent light by a factor of 100 (Sutter Lambda LS 300W Light Source). Complete lineage analysis was performed on assembled image stacks. The fluorescent signal from each cell was measured after background subtraction and manual annotation of regions of interest using ImageJ. The fluorescence signal from the first founding specified cell in each lineage (F) was used as a point of normalization to all derivative cells in the lineage. To calculate ΔF/F, F was subtracted from the signal from each cell, then divided by F. Using this approach, the change in signal through time in different cell types is readily apparent.

SUPPLEMENTAL DATA

The Supplemental Data include ten figures, one table, Supplemental Experimental Procedures, and four movies and can be found with this article online at http://www.molecule.org/supplemental/S1934-5909(08)00482-7.

ACKNOWLEDGMENTS

Several students contributed to the manual annotation of lineages in development of this project, including Daniel Ahmad, Kathleen Bandt, Elizabeth Baumel, Vince Beachley, Pavana Beerelli, Alissa Berliner, Sarah Gan, Brinda Gupta, Daniel Holohan, Josh Lieberman, Reut Mushkat, Christopher Nabel, Meghan Nelson, Emily Prentice, Nicole Ramsey, Jean Suh, and Sahar Zadeh.

Professors Ralf Schnabel and Anja-Kristin Schulz provided a script for extracting data from SIMI® BioCell. The authors thank Kang Li and Takeo Kanade (Carnegie Mellon University) for the image stabilizer plugin to ImageJ and Wayne Rasband (NIH) for supporting ImageJ. This research was supported by the Intramural Research Program of the NIH, NINDS.

Received: August 28, 2007
Revised: April 11, 2008
Accepted: September 18, 2008
Published: December 3, 2008

REFERENCES

Barnabe-Heider, F., Wasylnka, J.A., Fernandes, K.J., Porsche, C., Sendtner, M., Kaplan, D.R., and Miller, F.D. (2005). Evidence that embryonic neurons regulate the onset of cortical gliogenesis via cardiotrophin-1. Neuron *48*, 253–265.

Blondel, O., Collin, C., McCarran, W.J., Zhu, S., Zamostiano, R., Gozes, I., Brenneman, D.E., and McKay, R.D. (2000). A glia-derived signal regulating neuronal differentiation. J. Neurosci. *20*, 8012–8020.

Bonni, A., Sun, Y., Nadal-Vicens, M., Bhatt, A., Frank, D.A., Rozovsky, I., Stahl, N., Yancopoulos, G.D., and Greenberg, M.E. (1997). Regulation of gliogenesis in the central nervous system by the JAK-STAT signaling pathway. Science *278*, 477–483.

Capela, A., and Temple, S. (2002). LeX/ssea-1 is expressed by adult mouse CNS stem cells, identifying them as nonependymal. Neuron *35*, 865–875.

Capela, A., and Temple, S. (2006). LeX is expressed by principle progenitor cells in the embryonic nervous system, is secreted into their environment and binds Wnt-1. Dev. Biol. *291*, 300–313.

Cattaneo, E., and McKay, R. (1990). Proliferation and differentiation of neuronal stem cells regulated by nerve growth factor. Nature *347*, 762–765.

Caviness, V.S., Jr., Takahashi, T., and Nowakowski, R.S. (1995). Numbers, time and neocortical neuronogenesis: a general developmental and evolutionary model. Trends Neurosci. *18*, 379–383.

Chenn, A., and McConnell, S.K. (1995). Cleavage orientation and the asymmetric inheritance of Notch1 immunoreactivity in mammalian neurogenesis. Cell *82*, 631–641.

Davis, A.A., and Temple, S. (1994). A self-renewing multipotential stem cell in embryonic rat cerebral cortex. Nature *372*, 263–266.

Doetsch, F., Caille, I., Lim, D.A., Garcia-Verdugo, J.M., and Alvarez-Buylla, A. (1999). Subventricular zone astrocytes are neural stem cells in the adult mammalian brain. Cell *97*, 703–716.

Fasano, C.A., Dimos, J.T., Ivanova, N.B., Lowry, N., Lemischka, I.R., and Temple, S. (2007). shRNA knockdown of Bmi-1 reveals a critical role for p21-Rb pathway in NSC self-renewal during development. Cell Stem Cell *1*, 87–99.

Fukuda, S., Abematsu, M., Mori, H., Yanagisawa, M., Kagawa, T., Nakashima, K., Yoshimura, A., and Taga, T. (2007). Potentiation of astrogliogenesis by STAT3-mediated activation of bone morphogenetic protein-Smad signaling in neural stem cells. Mol. Cell. Biol. *27*, 4931–4937.

Hanna, J., Markoulaki, S., Schorderet, P., Carey, B.W., Beard, C., Wernig, M., Creyghton, M.P., Steine, E.J., Cassady, J.P., Foreman, R., et al. (2008). Direct reprogramming of terminally differentiated mature B lymphocytes to pluripotency. Cell *133*, 250–264.

Johe, K.K., Hazel, T.G., Muller, T., Dugich-Djordjevic, M.M., and McKay, R.D. (1996). Single factors direct the differentiation of stem cells from the fetal and adult central nervous system. Genes Dev. *10*, 3129–3140.

Lu, B., Jan, L., and Jan, Y.N. (2000). Control of cell divisions in the nervous system: symmetry and asymmetry. Annu. Rev. Neurosci. *23*, 531–556.

Morrison, S.J., and Kimble, J. (2006). Asymmetric and symmetric stem-cell divisions in development and cancer. Nature *441*, 1068–1074.

Nakashima, K., Yanagisawa, M., Arakawa, H., Kimura, N., Hisatsune, T., Kawabata, M., Miyazono, K., and Taga, T. (1999). Synergistic signaling in fetal brain by STAT3-Smad1 complex bridged by p300. Science *284*, 479–482.

Noctor, S.C., Martinez-Cerdeno, V., Ivic, L., and Kriegstein, A.R. (2004). Cortical neurons arise in symmetric and asymmetric division zones and migrate through specific phases. Nat. Neurosci. *7*, 136–144.

Ogawa, M. (1993). Differentiation and proliferation of hematopoietic stem cells. Blood *81*, 2844–2853.

Osawa, M., Hanada, K., Hamada, H., and Nakauchi, H. (1996). Long-term lymphohematopoietic reconstitution by a single CD34-low/negative hematopoietic stem cell. Science *273*, 242–245.

Panchision, D.M., Chen, H.L., Pistollato, F., Papini, D., Ni, H.T., and Hawley, T.S. (2007). Optimized flow cytometric analysis of central nervous system tissue reveals novel functional relationships among cells expressing CD133, CD15, and CD24. Stem Cells *25*, 1560–1570.

Qian, X., Shen, Q., Goderie, S.K., He, W., Capela, A., Davis, A.A., and Temple, S. (2000). Timing of CNS cell generation: a programmed sequence of neuron and glial cell production from isolated murine cortical stem cells. Neuron *28*, 69–80.

Rajan, P., and McKay, R.D. (1998). Multiple routes to astrocytic differentiation in the CNS. J. Neurosci. *18*, 3620–3629.

Schnabel, R., Hutter, H., Moerman, D., and Schnabel, H. (1997). Assessing normal embryogenesis in Caenorhabditis elegans using a 4D microscope: variability of development and regional specification. Dev. Biol. *184*, 234–265.

Shen, Q., Wang, Y., Dimos, J.T., Fasano, C.A., Phoenix, T.N., Lemischka, I.R., Ivanova, N.B., Stifani, S., Morrisey, E.E., and Temple, S. (2006). The timing of cortical neurogenesis is encoded within lineages of individual progenitor cells. Nat. Neurosci. *9*, 743–751.

Slack, J.M.W. (1991). From Egg To Embryo, Second Edition (Cambridge: Cambridge University Press).

Song, H.J., Stevens, C.F., and Gage, F.H. (2002). Neural stem cells from adult hippocampus develop essential properties of functional CNS neurons. Nat. Neurosci. *5*, 438–445.

Song, M.R., and Ghosh, A. (2004). FGF2-induced chromatin remodeling regulates CNTF-mediated gene expression and astrocyte differentiation. Nat. Neurosci. *7*, 229–235.

Spangrude, G.J., Heimfeld, S., and Weissman, I.L. (1988). Purification and characterization of mouse hematopoietic stem cells. Science *241*, 58–62.

Sun, Y., Goderie, S.K., and Temple, S. (2005). Asymmetric distribution of EGFR receptor during mitosis generates diverse CNS progenitor cells. Neuron *45*, 873–886.

Takahashi, K., and Yamanaka, S. (2006). Induction of pluripotent stem cells from mouse embryonic and adult fibroblast cultures by defined factors. Cell *126*, 663–676.

Till, J.E., McCulloch, E.A., and Siminovitch, L. (1964). A Stochastic Model of Stem Cell Proliferation, Based on the Growth of Spleen Colony-Forming Cells. Proc. Natl. Acad. Sci. USA *51*, 29–36.

Uchida, N., Buck, D.W., He, D., Reitsma, M.J., Masek, M., Phan, T.V., Tsukamoto, A.S., Gage, F.H., and Weissman, I.L. (2000). Direct isolation of human central nervous system stem cells. Proc. Natl. Acad. Sci. USA *97*, 14720–14725.

Vicario-Abejon, C., Collin, C., McKay, R.D., and Segal, M. (1998). Neurotrophins induce formation of functional excitatory and inhibitory synapses between cultured hippocampal neurons. J. Neurosci. *18*, 7256–7271.

Weissman, I.L. (1994). Stem cells, clonal progenitors, and commitment to the three lymphocyte lineages: T, B, and NK cells. Immunity *1*, 529–531.